




# V0644 Ser: An Active Ultrashort Period Contact Binary Star

Hu-Shan Xu<sup>1,2</sup>, Li-Ying Zhu<sup>1,2,3</sup>, Sarotsakulchai Thawicharat<sup>4</sup> , and Soonthornthum Boonruksar<sup>4</sup>

<sup>1</sup>Yunnan Observatories, Chinese Academy of Sciences (CAS), Kunming 650216, China; [xuhushan@ynao.ac.cn](mailto:xuhushan@ynao.ac.cn)

<sup>2</sup>University of the Chinese Academy of Sciences, Beijing 100049, China

<sup>3</sup>Key Laboratory of the Structure and Evolution of Celestial Objects, Chinese Academy of Sciences, Kunming 650216, China

<sup>4</sup>National Astronomical Research Institute of Thailand, 191 Siriphanich Bldg., Huay Kaew Rd., Chiang Mai 50200, Thailand

Received 2021 December 9; revised 2022 January 12; accepted 2022 January 14; published 2022 February 25

## Abstract

The photometric solutions of the ultrashort period close binary V0644 Ser based on our new complete *BVRI* light curves are derived by the Wilson–Devinney code. The results show that V0644 Ser is a W-type shallow contact binary, and the third light was found in the *R* and *I* bands. Compared with the light curves in 2011, the amplitude variation of the secondary maximum can be explained by the temperature change from hot to cold in the local region of the star surface caused by magnetic activity or convective instability. Combined with the Gaia parallax, the absolute parameters of this system are obtained:  $M_1 = 0.29(4) M_\odot$ ,  $M_2 = 0.56(9) M_\odot$ ,  $R_1 = 0.48(3) R_\odot$ ,  $R_2 = 0.65(3) R_\odot$ ,  $L_1 = 0.11(2) L_\odot$ ,  $L_2 = 0.16(2) L_\odot$ . To study the period variation, we fitted the SuperWASP, CSS, ASAS-SN and ZTF survey timing data to obtain light minima times spanning 14 yr. Through *O* – *C* analysis, we find that the orbital period of this system has a long-term period decrease and periodic oscillation. The long-term period decrease can be explained by the mass transfer from more-massive component to less one and angular momentum loss via magnetic stellar wind. With the period decrease, this system is evolving from the present shallow contact phase to a relatively deeper stage predicted by the thermal relaxation oscillation theory. Periodic oscillation can be explained by the light-time effect of the cool third body. This third body may play an important role in the early formation and evolution of the binary system by removing angular momentum.

*Key words:* (stars:) binaries (including multiple): close – (stars:) binaries: eclipsing – stars: late-type – stars: individual (..., ...)

## 1. Introduction

W UMa contact binaries are late-type contact binaries with both components filling their critical Roche lobes (Kopal 1959) and sharing a convective common envelope (Lucy 1968). Their two components have almost equal effective temperatures. Since this class of stars consists of two late-type stars, the O’Connell effect (primary and secondary maximum unequal height) (O’Connell 1951) caused by magnetic activity is often observed. Binnendijk (1970) divided them into two subtypes according to their light curve, A-type and W-type. A-type is characterized by a higher surface temperature of more-massive component, whereas W-type is the opposite. W UMa contact binaries have a period cutoff at about 0.22 days. Rucinski (1992) proposed that the fully convective limit can possibly explain the period cutoff. Stepien (2006) suggested that the timescale of the angular momentum loss (AML) is too long to form such short period contact binaries. Jiang et al. (2012) also theoretically suggested the contact binaries under the period limit should be unstable that they are rapidly destroyed. Li et al. (2019) suggested that both the fully convective limit and angular momentum loss theory could produce period cutoff by studying the period-color and color-density relationships of ultrashort period contact binaries. Qian et al. (2017) suggested a lower period cutoff at about 0.2 days by showing the period

distribution of EW-type binaries based on the LAMOST data. Zhang & Qian (2020) predicted a period cutoff at about 0.15 days theoretically by studying the correlation among physical parameters of contact binaries. Recently, some contact binaries around the cutoff have indeed been observed, such as SDSS J001641-000925 (Davenport et al. 2013), 1SWASP J015100.23-100524.2 (Qian et al. 2015), NSVS 8626028 (Dimitrov & Kjurkchieva 2015), CSS J214633.8+120016 (Kjurkchieva et al. 2016), CRTS J145224.5+011522 (Li et al. 2020), etc. Qian et al. (2015) suggested that the third body may play an important role for the origin and evolution of this short period contact binaries by removing angular momentum from the central binary system. However, such the ultrashort period contact binaries are too rare to obtain more statistical information. Studying the ultrashort period contact binaries can shed light on the rarity of them, and their origin and evolution. In addition, W UMa contact binaries usually exhibit EW light curves, and the eclipse depth difference of the primary minima and the secondary minima is almost equal. However, there are some contact binary systems whose light curves deviate from EW-type to EB-type, and show shallow contact characteristics. They are good targets for testing the thermal relaxation oscillation theory

(TRO theory; e.g., Flannery 1976; Lucy 1976; Robertson & Eggleton 1977; Wilson 1979).

V0644 Ser (=ISWASP J153951.12+105420.7) was first discovered to be an eclipsing binary candidate with a period of 19,070.320 s (0.2207213 days) by SuperWASP project (Lohr et al. 2013). Its difference of eclipse depth between the primary minima and the secondary minima is 0.15 in *V* mag. Based on the preliminary *O* – *C* analysis for SuperWASP data, there may be a secular decreasing trend in the period of this system, or the trend is part of the periodic oscillations of the system. Unfortunately, the time span of the *O* – *C* data is only about five years, which makes further analysis impossible. Kjurkchieva et al. (2018) presented photometric and the low-resolution spectroscopic observations, and determined the temperature of the primary component as 4750 K for this system. They carried out the modeling of *VI* light curves by the package PHOEBE, and concluded that V0644 Ser is a W UMa contact system composed of two late-type stars ( $M_1 = 0.74M_\odot$ ;  $M_2 = 0.34M_\odot$ ). In this paper, combined our new *BVRI* light curves, we analyzed all light curves of this system, and found that the secondary maximum has changed. Then, we collected more timings data spanning more than 14 yr and analyzed the period variation of V0644 Ser. Finally, we discussed the structure and evolution of the system.

## 2. Observation

We have monitored V0644 Ser with the 85 cm reflecting telescope at Xinglong Station of the National Astronomical Observatories, Chinese Academy of Sciences (NAOC) on 2019 May 30. The telescope is equipped with CCD cameras and the standard Johnson-Cousin *BVRI* filters. The integration times for different filters are 40 to 60 s (*B*), 25 to 30 s (*V*), 10 to 15 s (*R*) and 15 s (*I*) according to the weather conditions during the observations. The adopted CCD images were processed by using the IRAF (Image Reduction and Analysis Facility) software and the method of differential photometry. Two stars that are very close in distance and brightness were chosen as the comparison star ( $\alpha_{2000} = 15^{\text{h}}39^{\text{m}}54^{\text{s}}.78 + 10^{\circ}55'57''.29$ ) and check star ( $\delta_{2000} = 15^{\text{h}}40^{\text{m}}15^{\text{s}}.10 + 10^{\circ}57'33''.46$ ). The photometric four-color light curves of V0644 Ser are shown in Figure 1. The standard deviations of the differential magnitude between the check star and the comparison star for each band are used to evaluate the errors of the data, which are 0.011 mag for the *I* band, 0.012 mag for the *R* band, 0.012 mag for the *V* band and 0.014 mag for the *B* band, respectively. Based on the observations, three new times of light minima were obtained for the binary system, which are listed in Table 1.

As shown in Figure 1, the light curves of V0644 Ser are EB-type, which show the difference of eclipse depth between the primary and secondary minima exceeds 0.1 mag. This indicates that there is a relatively larger temperature difference between two components of this system comparing with the EW-type. In order to compare the changes in light curves observed in different years,

we summarized the information about the light levels of the light curves in different bands of V0644 Ser on 2011 and 2019, which are listed in Table 2. From Table 2, the difference of eclipse depth between the primary and secondary minima of the light curves in different wavelength is different. From the longer wavelength to the shorter one, the amplitude of the light variation become larger for shorter wavelengths, which may implies that the existence of a cool third body because the radiation of the lower temperature third body concentrates on the longer wavelength. In addition, there is an O’Connell effect (O’Connell 1951) with the secondary maximum higher than the primary one in 2011. The differential magnitudes between the primary maximum and the secondary maximum in the *V* band (shorter wavelength) is higher than that in the *I* band (longer wavelength). However, the change is different in 2019, which the primary maximum higher than the secondary one. The primary maximum profiles in 2011 and 2019 are consistent in different bands, which means that the luminosity in the primary maximum is the same, and the system is in a stable state around the 0.5 phase. In order to compare the changes of light curves in 2011 and 2019 more intuitively, we took the magnitude of the primary minimum for the *V* band and *I* band in 2011 as the reference, and shifted the *V* band and *I* band in 2019 to the same magnitude of the primary minimum for the corresponding band, which are shown in Figure 2. It can be clearly seen from Figure 2 that the primary maximum in 2011 is almost the same height as 2019. But the secondary maximum in 2011 is higher than 2019.

## 3. Analysis of Photometric Data

### 3.1. Analysis of *O* – *C*

The analysis of *O* – *C* curve is an important method to understand the period variation of V0644 Ser. However, there are very few timing observations on this system. Beside the three new times of light minima obtained by our observations, we have derived three minimum times by fitting the eclipse profiles from Kjurkchieva et al. (2018). In addition, the useful data observed by the SuperWASP Survey covering from 2008 to 2014 provided by Prof. Norton. For other sky survey missions with low time resolution, such as the Catalina Sky Survey (CSS, Drake et al. 2014), the All-Sky Automated Survey for SuperNova (ASAS-SN, Shappee et al. 2014) and the Zwicky Transient Facility (ZTF, Graham et al. 2019; Masci et al. 2019), we used the mean minimum time method (Li et al. 2021a) to obtain the complete light curve. Based on all these data, 206 light minimum times are obtained by parabolic fitting and listed in Table 3. The *O* – *C* values with respect to the following linear ephemeris

$$\text{Min.I(HJD)} = 2,458,634.18498 + 0^{\text{d}}.2207213 \times E \quad (1)$$

were computed. The corresponding (*O* – *C*)<sub>1</sub> diagram is shown in the upper panel of Figure 3, where open circles refer to data derived from Kjurkchieva et al. (2018), and solid dots and triangle represents our new observations and SuperWASP data,

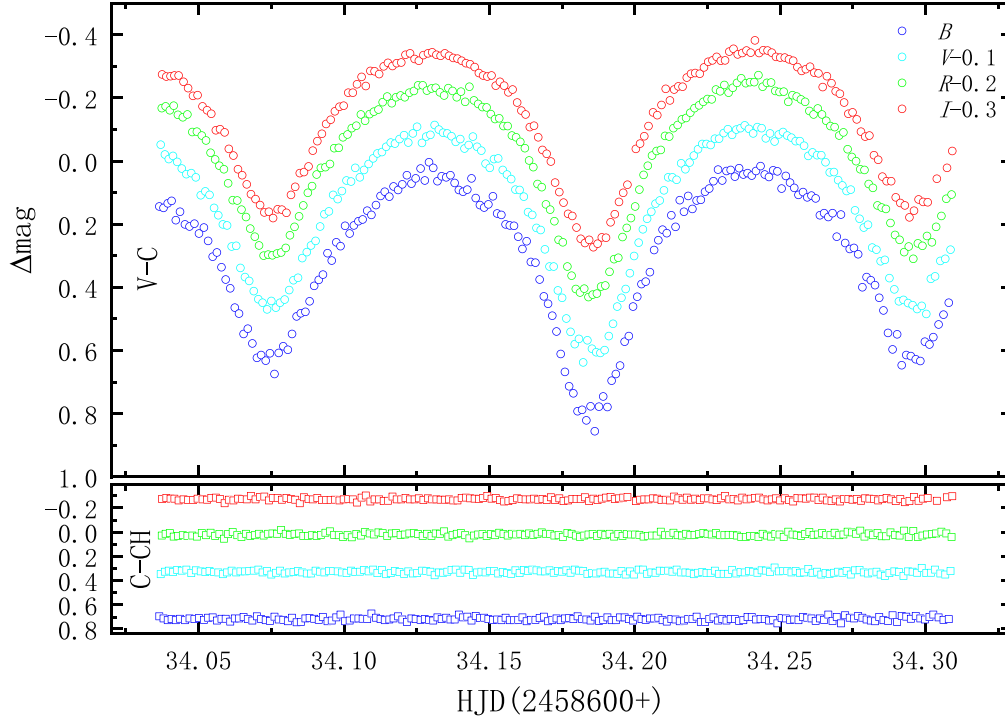


**Figure 1.** The light curves of V0644 Ser observed by Xinglong 85 cm telescope on 2019 May 30.

**Table 1**  
New Times of Light Minima of V0644 Ser

Time of minimum [HJD](Errors)	Filters	Type
2,458,634.18498(22)	<i>B</i>	I
2,458,634.07476(25)	<i>B</i>	II
2,458,634.29571(30)	<i>B</i>	II
2,458,634.18498(23)	<i>V</i>	I
2,458,634.07503(15)	<i>V</i>	II
2,458,634.29536(32)	<i>V</i>	II
2,458,634.18478(17)	<i>R</i>	I
2,458,634.07530(11)	<i>R</i>	II
2,458,634.29559(29)	<i>R</i>	II
2,458,634.18519(15)	<i>I</i>	I
2,458,634.07513(19)	<i>I</i>	II
2,458,634.29555(26)	<i>I</i>	II

**Note.** One set of primary minimum and two sets of secondary minimum are obtained. I and II refer to the primary minimum and secondary minimum, respectively.

respectively. Squares, inverted triangles, and diamonds represent light minima from CSS, ASAS-AN, and ZTF respectively. There was weak evidence (the changes significant at  $1\sigma$ ) that the period of V0644 Ser is decreasing (Lohr et al. 2013). Therefore, parabola is used to fit the  $O - C$  values, the theoretical curve is shown in the upper panel of Figure 3, and the residuals ( $O - C$ )<sub>2</sub> are shown in the middle panel. As can be seen from the upper

**Table 2**  
The Differences of Light Levels in the Light Curves of V0644 Ser

Year	Type				
		$\Delta B$	$\Delta V$	$\Delta R$	$\Delta I$
2011	minI-minII	...	0.187	...	0.114
	maxI-maxII	...	0.033	...	0.025
	minI-maxI	...	0.707	...	0.607
	minI-maxII	...	0.740	...	0.632
2019	minI-minII	0.178	0.145	0.130	0.099
	maxI-maxII	-0.013	-0.013	-0.017	-0.013
	minI-maxI	0.772	0.706	0.671	0.610
	minI-maxII	0.758	0.693	0.654	0.597

**Note.** I and II refer to the primary and the secondary, respectively.

panel of Figure 3, there is also a periodic oscillation in the residuals ( $O - C$ )<sub>2</sub>. So we add a sine term to fit the residuals ( $O - C$ )<sub>2</sub>. The result is the following ephemeris,

$$\begin{aligned} \text{MinI} = & \text{HJD}2,458,634.1864(8) + 0.2207199(1)E \\ & - 6.7(2) \times 10^{-11}E^2 \\ & + 0.0029(1) \times \sin(0.024(1)\text{deg}E + 236(3)\text{deg}). \end{aligned} \quad (2)$$

The quadratic term in Equation (2) reveals a long period decrease at a rate of  $dP/dt = 2.23(\pm 0.07) \times 10^{-7}$  days  $\text{yr}^{-1}$ .

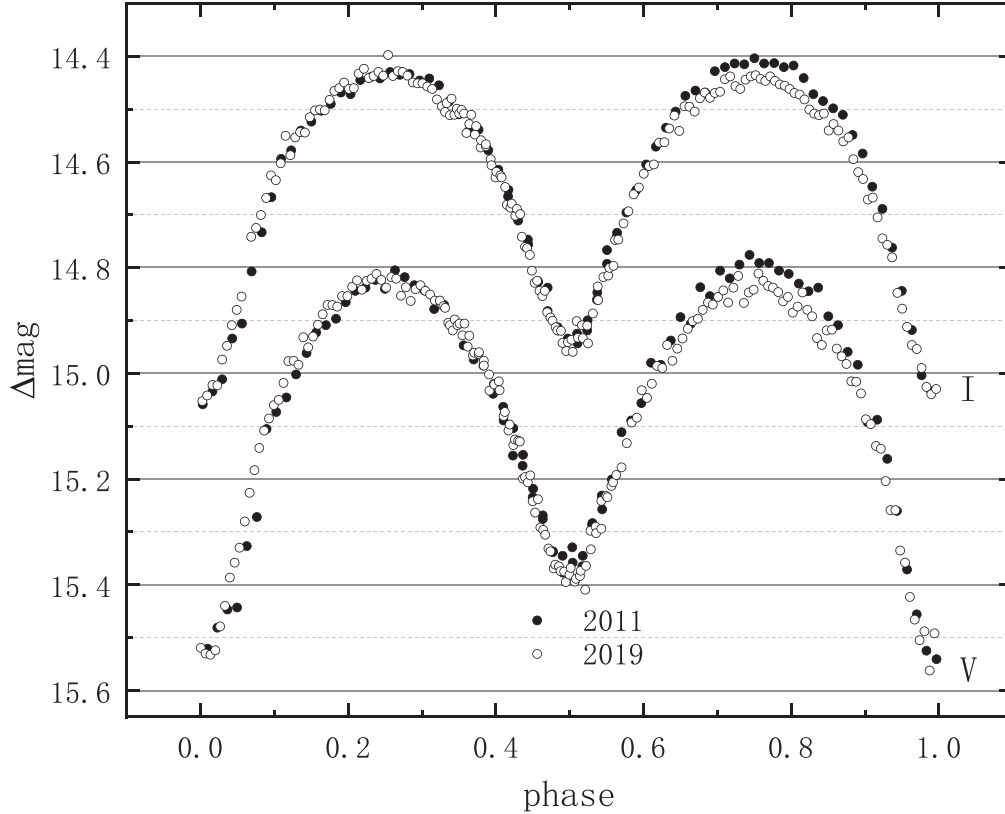


**Figure 2.** The diagram of shape of light curves in the VI band of V0644 ser in 2011 and 2019.

The sinusoidal term implies a periodic change with an amplitude of 0.0029 days and a period of 9.15 yr.

### 3.2. Analysis with the W-D Method

Comparing the two-sets light curves, the O’Connell effect was positive in 2011 and negative in 2019. In order to obtain more accurate photometric solution, We employed the Wilson–Devinney (W-D) (2013 version) method (Wilson & Devinney 1971; Wilson 1990, 1994) to analyze our four-color light curves and VI light curves of Kjurkchieva et al. (2018) at the same time. The temperature for star 1 was fixed as  $T_1 = 4750$  K. As the components of V0644 Ser are late-type stars, the gravity-darkening coefficients  $g_1 = g_2 = 0.32$  and the bolometric albedo  $A_1 = A_2 = 0.5$  were applied. The square-root bolometric and bandpass limb-darkening parameters are taken from Van Hamme (1993).

Since the mass ratio is unknown, we search the photometric mass ratio by the q-search method. During the photometric solution, we tried different configurations, i.e., detached (mode 2), contact (mode 3), semi-detached (mode 4 and mode 5). Finally, we found the convergent solution at contact configurations (model 3). The adjustable parameters are the orbital inclination  $i$ ; the surface effective temperature of star 2,  $T_2$ ; the monochromatic luminosity

of star 1,  $L_1$ ; and the dimensionless potential  $\Omega$  ( $\Omega_1 = \Omega_2$  for mode 3). We search the mass ratio in the range from 0.1 to 5 with the step size 0.1 (near the bottom 0.05) at first, and the converged solutions and corresponding resulting sum of weighted square deviations are collected. Their relationships are plotted in Figure 4. From Figure 4, we can see that the minimum  $\Sigma$  corresponding to the mass ratio is 1.95. Then choosing  $q = 1.95$  as the initial value and releasing it as an adjustable parameter, we derived the final converged solutions for the two-sets light curves after a differential correction. The corresponding photometric parameters are listed in column 2 of Table 4. The theoretical curves (dotted lines) are shown in the upper panel of Figure 5. Then, we use this solutions as the basic solutions (fix the parameters of the solutions) and add a spot on the surface of the star to fit the light curves. Since the primary maximum of the light curves in 2011 and 2019 is the same shape, the spot activity is most likely to occur around the 0.75 phase. By experiment, a spot was added to the surface of star 1 near the 0.75 phase. It was a hot spot in 2011 and a cool spot in 2019. The results are listed in columns 3 and 4 of Table 4, and the theoretical curve (solid lines) is shown in the upper panel of Figure 5. The spot parameters are latitude ( $\phi$ ), longitude ( $\theta$ ), angular radius ( $r_s$ ), and the temperature factor ( $T_f = T_s/T_e$ ;  $T_f$  is the ratio between the spot temperature  $T_s$  and the surface effective temperature  $T_e$  of star). The geometrical structure with spot of

**Table 3**  
All Available times of Light Minima of V0644 Ser

HJD	Errors	$E$	$O - C$	source	HJD	Errors	$E$	$O - C$	source
2,454,558.68186	0.00094	-18464.5	0.00532	SuperWASP	2,455,377.44128	0.00311	-14755	-0.00092	SuperWASP
2,454,571.59855	0.00230	-18406	0.00982	SuperWASP	2,455,378.43859	0.00103	-14750.5	0.00314	SuperWASP
2,454,573.57165	0.00243	-18397	-0.00358	SuperWASP	2,455,379.43463	0.00129	-14746	0.00594	SuperWASP
2,454,573.69060	0.00444	-18396.5	0.00501	SuperWASP	2,455,646.72920	0.00127	-13535	0.00701	SuperWASP
2,454,575.56903	0.00576	-18388	0.00731	SuperWASP	2,455,647.72718	0.00137	-13530.5	0.01175	SuperWASP
2,454,591.67769	0.00125	-18315	0.00332	SuperWASP	2,455,648.71638	0.00159	-13526	0.00770	SuperWASP
2,454,597.64051	0.00098	-18288	0.00666	SuperWASP	2,455,649.70657	0.00194	-13521.5	0.00465	SuperWASP
2,454,616.61821	0.00126	-18202	0.00233	SuperWASP	2,456,434.48891	0.00135	-9966	0.01240	SuperWASP
2,454,619.60282	0.00053	-18188.5	0.00720	SuperWASP	2,456,434.60083	0.00186	-9965.5	0.01396	SuperWASP
2,454,621.47735	0.00129	-18180	0.00560	SuperWASP	2,456,435.48338	0.00191	-9961.5	0.01363	SuperWASP
2,454,623.46147	0.00083	-18171	0.00323	SuperWASP	2,456,435.58644	0.00163	-9961	0.00633	SuperWASP
2,454,624.45837	0.00081	-18166.5	0.00688	SuperWASP	2,456,443.53117	0.00056	-9925	0.00509	SuperWASP
2,454,625.45690	0.01090	-18162	0.01217	SuperWASP	2,456,444.52906	0.00095	-9920.5	0.00973	SuperWASP
2,454,626.44564	0.00082	-18157.5	0.00766	SuperWASP	2,456,445.41627	0.00094	-9916.5	0.01406	SuperWASP
2,454,627.43724	0.00231	-18153	0.00602	SuperWASP	2,456,445.52085	0.00042	-9916	0.00828	SuperWASP
2,454,628.42845	0.00184	-18148.5	0.00398	SuperWASP	2,456,445.63008	0.00084	-9915.5	0.00715	SuperWASP
2,454,629.42324	0.00108	-18144	0.00552	SuperWASP	2,456,446.40681	0.00063	-9912	0.01135	SuperWASP
2,454,630.42031	0.00211	-18139.5	0.00935	SuperWASP	2,456,446.51673	0.00061	-9911.5	0.01091	SuperWASP
2,454,636.49578	0.00993	-18112	0.01498	SuperWASP	2,456,446.62291	0.00062	-9911	0.00673	SuperWASP
2,454,638.46765	0.00230	-18103	0.00036	SuperWASP	2,456,447.40331	0.00106	-9907.5	0.01461	SuperWASP
2,454,639.46713	0.00272	-18098.5	0.00660	SuperWASP	2,456,447.50692	0.00051	-9907	0.00786	SuperWASP
2,454,640.45910	0.00061	-18094	0.00532	SuperWASP	2,456,447.62131	0.00065	-9906.5	0.01189	SuperWASP
2,454,642.44620	0.00080	-18085	0.00593	SuperWASP	2,456,449.49300	0.00048	-9898	0.00744	SuperWASP
2,454,644.43216	0.00113	-18076	0.00540	SuperWASP	2,456,449.60491	0.00073	-9897.5	0.00899	SuperWASP
2,454,646.41768	0.00124	-18067	0.00442	SuperWASP	2,456,450.49040	0.00059	-9893.5	0.01160	SuperWASP
2,454,647.52290	0.00171	-18062	0.00604	SuperWASP	2,456,450.59772	0.00061	-9893	0.00856	SuperWASP
2,454,921.66179	0.00128	-16820	0.00907	SuperWASP	2,456,451.48089	0.00048	-9889	0.00884	SuperWASP
2,454,925.63618	0.00133	-16802	0.01048	SuperWASP	2,456,451.59251	0.00056	-9888.5	0.01010	SuperWASP
2,454,926.73353	0.00091	-16797	0.00422	SuperWASP	2,456,452.47440	0.00050	-9884.5	0.00911	SuperWASP
2,454,927.72900	0.00131	-16792.5	0.00645	SuperWASP	2,456,452.58302	0.00048	-9884	0.00737	SuperWASP
2,454,928.71881	0.00567	-16788	0.00301	SuperWASP	2,456,453.46729	0.00046	-9880	0.00875	SuperWASP
2,454,930.71041	0.00356	-16779	0.00812	SuperWASP	2,456,453.57924	0.00048	-9879.5	0.01034	SuperWASP
2,454,936.66655	0.00329	-16752	0.00479	SuperWASP	2,456,454.46461	0.00064	-9875.5	0.01283	SuperWASP
2,454,938.65266	0.00131	-16743	0.00440	SuperWASP	2,456,454.57035	0.00050	-9875	0.00821	SuperWASP
2,454,949.68875	0.00101	-16693	0.00443	SuperWASP	2,456,455.45142	0.00057	-9871	0.00639	SuperWASP
2,454,950.68520	0.00248	-16688.5	0.00763	SuperWASP	2,456,455.56465	0.00064	-9870.5	0.00926	SuperWASP
2,454,953.66215	0.00098	-16675	0.00485	SuperWASP	2,456,456.45064	0.00055	-9866.5	0.01236	SuperWASP
2,454,955.65288	0.00070	-16666	0.00908	SuperWASP	2,456,456.55551	0.00046	-9866	0.00687	SuperWASP
2,454,956.64557	0.00288	-16661.5	0.00853	SuperWASP	2,456,457.43973	0.00072	-9862	0.00821	SuperWASP
2,454,958.51426	0.00178	-16653	0.00109	SuperWASP	2,456,457.55351	0.00065	-9861.5	0.01163	SuperWASP
2,454,958.62392	0.00200	-16652.5	0.00039	SuperWASP	2,456,458.43707	0.00083	-9857.5	0.01230	SuperWASP
2,454,969.55445	0.00096	-16603	0.00521	SuperWASP	2,456,458.54388	0.00059	-9857	0.00875	SuperWASP
2,454,973.63890	0.00081	-16584.5	0.00632	SuperWASP	2,456,459.42758	0.00055	-9853	0.00957	SuperWASP
2,454,975.51253	0.00109	-16576	0.00382	SuperWASP	2,456,459.54261	0.00069	-9852.5	0.01424	SuperWASP
2,454,977.50152	0.00167	-16567	0.00631	SuperWASP	2,456,460.41623	0.00099	-9848.5	0.00497	SuperWASP
2,454,978.49546	0.00161	-16562.5	0.00701	SuperWASP	2,456,460.53022	0.00072	-9848	0.00860	SuperWASP
2,454,979.48901	0.00144	-16558	0.00731	SuperWASP	2,456,461.41257	0.00077	-9844	0.00806	SuperWASP
2,454,981.58450	0.00183	-16548.5	0.00595	SuperWASP	2,456,461.52373	0.00082	-9843.5	0.00886	SuperWASP
2,454,982.57984	0.00132	-16544	0.00804	SuperWASP	2,456,462.40978	0.00135	-9839.5	0.01203	SuperWASP
2,454,983.58079	0.00151	-16539.5	0.01575	SuperWASP	2,456,462.51318	0.00123	-9839	0.00507	SuperWASP
2,454,985.43752	0.00171	-16531	-0.00365	SuperWASP	2,456,463.50977	0.00131	-9834.5	0.00841	SuperWASP
2,454,986.44043	0.00167	-16526.5	0.00601	SuperWASP	2,456,468.47397	0.00120	-9812	0.00638	SuperWASP
2,454,987.43368	0.00186	-16522	0.00602	SuperWASP	2,456,469.47371	0.00145	-9807.5	0.01288	SuperWASP
2,454,991.40780	0.00284	-16504	0.00715	SuperWASP	2,456,469.57153	0.00199	-9807	0.00034	SuperWASP
2,454,992.40263	0.00146	-16499.5	0.00874	SuperWASP	2,456,470.45769	0.00077	-9803	0.00361	SuperWASP
2,454,996.48103	0.00202	-16481	0.00379	SuperWASP	2,456,470.56817	0.00131	-9802.5	0.00373	SuperWASP
2,454,997.47657	0.00148	-16476.5	0.00609	SuperWASP	2,456,471.45706	0.00084	-9798.5	0.00974	SuperWASP
2,455,005.42838	0.00121	-16440.5	0.01193	SuperWASP	2,456,472.45072	0.00058	-9794	0.01015	SuperWASP



**Table 3**  
(Continued)

HJD	Errors	$E$	$O - C$	source	HJD	Errors	$E$	$O - C$	source
2,455,006.41533	0.00063	-16436	0.00563	SuperWASP	2,456,472.55305	0.00213	-9793.5	0.00212	SuperWASP
2,455,007.51987	0.00169	-16431	0.00657	SuperWASP	2,456,474.43445	0.00041	-9785	0.00739	SuperWASP
2,455,009.50316	0.00090	-16422	0.00337	SuperWASP	2,456,474.54091	0.00089	-9784.5	0.00349	SuperWASP
2,455,010.50077	0.00100	-16417.5	0.00773	SuperWASP	2,456,475.43087	0.00057	-9780.5	0.01056	SuperWASP
2,455,012.48618	0.00170	-16408.5	0.00665	SuperWASP	2,456,475.53705	0.00096	-9780	0.00638	SuperWASP
2,455,013.48052	0.00326	-16404	0.00774	SuperWASP	2,456,476.42248	0.00042	-9776	0.00893	SuperWASP
2,455,281.65751	0.00275	-15189	0.00835	SuperWASP	2,456,476.53184	0.00094	-9775.5	0.00793	SuperWASP
2,455,282.75189	0.00226	-15184	-0.00087	SuperWASP	2,456,477.41965	0.00061	-9771.5	0.01285	SuperWASP
2,455,286.62343	0.00193	-15166.5	0.00804	SuperWASP	2,456,477.52243	0.00093	-9771	0.00527	SuperWASP
2,455,286.73334	0.00249	-15166	0.00759	SuperWASP	2,456,478.41185	0.00047	-9767	0.01180	SuperWASP
2,455,287.72572	0.00188	-15161.5	0.00673	SuperWASP	2,456,478.52070	0.00079	-9766.5	0.01029	SuperWASP
2,455,293.67316	0.00109	-15134.5	-0.00531	SuperWASP	2,456,479.40741	0.00079	-9762.5	0.01412	SuperWASP
2,455,295.67128	0.00141	-15125.5	0.00632	SuperWASP	2,456,479.50998	0.00081	-9762	0.00633	SuperWASP
2,455,297.65570	0.00076	-15116.5	0.00425	SuperWASP	2,456,480.50685	0.00077	-9757.5	0.00995	SuperWASP
2,455,304.60903	0.00167	-15085	0.00486	SuperWASP	2,456,481.49614	0.00066	-9753	0.00600	SuperWASP
2,455,308.58364	0.00080	-15067	0.00648	SuperWASP	2,456,482.49462	0.00071	-9748.5	0.01123	SuperWASP
2,455,309.68058	0.00208	-15062	-0.00018	SuperWASP	2,456,483.48473	0.00068	-9744	0.00809	SuperWASP
2,455,321.60460	0.00347	-15008	0.00489	SuperWASP	2,456,484.48187	0.00086	-9739.5	0.01199	SuperWASP
2,455,324.57916	0.00141	-14994.5	-0.00029	SuperWASP	2,456,485.47147	0.00071	-9735	0.00834	SuperWASP
2,455,331.64946	0.00261	-14962.5	0.00693	SuperWASP	2,456,486.46716	0.00074	-9730.5	0.01079	SuperWASP
2,455,333.63493	0.00120	-14953.5	0.00591	SuperWASP	2,456,487.45891	0.00067	-9726	0.00929	SuperWASP
2,455,334.62850	0.00125	-14949	0.00623	SuperWASP	2,456,729.70632	0.00152	-8628.5	0.01507	SuperWASP
2,455,335.62376	0.00092	-14944.5	0.00825	SuperWASP	2,456,733.67689	0.00155	-8610.5	0.01266	SuperWASP
2,455,336.61345	0.00194	-14940	0.00469	SuperWASP	2,456,734.66966	0.00123	-8606	0.01219	SuperWASP
2,455,337.61189	0.00171	-14935.5	0.00988	SuperWASP	2,456,742.62193	0.00127	-8570	0.01849	SuperWASP
2,455,341.46945	0.00293	-14918	0.00482	SuperWASP	2,456,742.71876	0.00104	-8569.5	0.00496	SuperWASP
2,455,342.46982	0.00335	-14913.5	0.01195	SuperWASP	2,456,743.60819	0.00094	-8565.5	0.01150	SuperWASP
2,455,351.51461	0.00147	-14872.5	0.00716	SuperWASP	2,456,743.71561	0.00049	-8565	0.00856	SuperWASP
2,455,352.50491	0.00123	-14868	0.00422	SuperWASP	2,455,705.43852	0.00027	-13269	0.00447	Kjurkchieva et al. (2018)
2,455,353.49411	0.00190	-14863.5	0.00017	SuperWASP	2,455,705.32753	0.00026	-13269.5	0.00384	Kjurkchieva et al. (2018)
2,455,354.49423	0.00105	-14859	0.00704	SuperWASP	2,455,705.54745	0.00017	-13268.5	0.00304	Kjurkchieva et al. (2018)
2,455,355.48730	0.00123	-14854.5	0.00687	SuperWASP	2,458,634.07506	0.00019	-0.5	0.00043	NAOC 85 cm
2,455,356.48041	0.00107	-14850	0.00673	SuperWASP	2,458,634.18498	0.00029	0	0.00000	NAOC 85 cm
2,455,359.45806	0.00125	-14836.5	0.00464	SuperWASP	2,458,634.29555	0.00018	0.5	0.00021	NAOC 85 cm
2,455,360.45191	0.00078	-14832	0.00525	SuperWASP	2,453,907.55302	0.00027	-21414.5	0.00431	CSS
2,455,361.44486	0.00130	-14827.5	0.00495	SuperWASP	2,453,907.66595	0.00053	-21414	0.00688	CSS
2,455,362.44047	0.00092	-14823	0.00732	SuperWASP	2,454,908.30017	0.00039	-16880.5	0.00109	CSS
2,455,364.42644	0.00175	-14814	0.00680	SuperWASP	2,454,908.41013	0.00047	-16880	0.00069	CSS
2,455,365.41905	0.00212	-14809.5	0.00616	SuperWASP	2,456,100.97339	0.00057	-11477	0.00676	CSS
2,455,365.52893	0.00117	-14809	0.00568	SuperWASP	2,457,020.50125	0.00073	-7311	0.00969	ASAS-SN
2,455,367.41306	0.00186	-14800.5	0.01368	SuperWASP	2,457,761.23572	0.00086	-3955	0.00348	ASAS-SN
2,455,369.50336	0.00183	-14791	0.00713	SuperWASP	2,458,532.43203	0.00023	-461	-0.00043	ZTF
2,455,373.46727	0.00420	-14773	-0.00195	SuperWASP	2,458,532.54375	0.00022	-460.5	0.00093	ZTF
2,455,375.46043	0.00328	-14764	0.00472	SuperWASP	2,459,178.80885	0.00038	2467.5	-0.00594	ZTF
2,455,376.44697	0.00315	-14759.5	-0.00199	SuperWASP	2,459,178.92025	0.00035	2468	-0.00490	ZTF

V0644 Ser in different years are shown in the lower panel of Figure 5. In addition, we also found the contribution of third light in the  $R$  band and  $I$  band, which are listed in Table 4.

## 4. Discussions and Conclusions

### 4.1. Photometric Solutions

The new four-color light curves of V0644 Ser were analyzed by the W-D code. The photometric solutions showed that

V0644 Ser is a W-type shallow contact binary system. The temperature of the primary component (more massive) is lower than that of the secondary component, and the contact degree  $f$  is about 0.14 in this system. Compared with the  $VI$  band light curves in 2011, we find that the secondary maximum has changed significantly in recent years, while that of the primary does not. The amplitude of this change is different at different wavelengths in different years, which implies that there is a region around the 0.75 phase where the temperature change

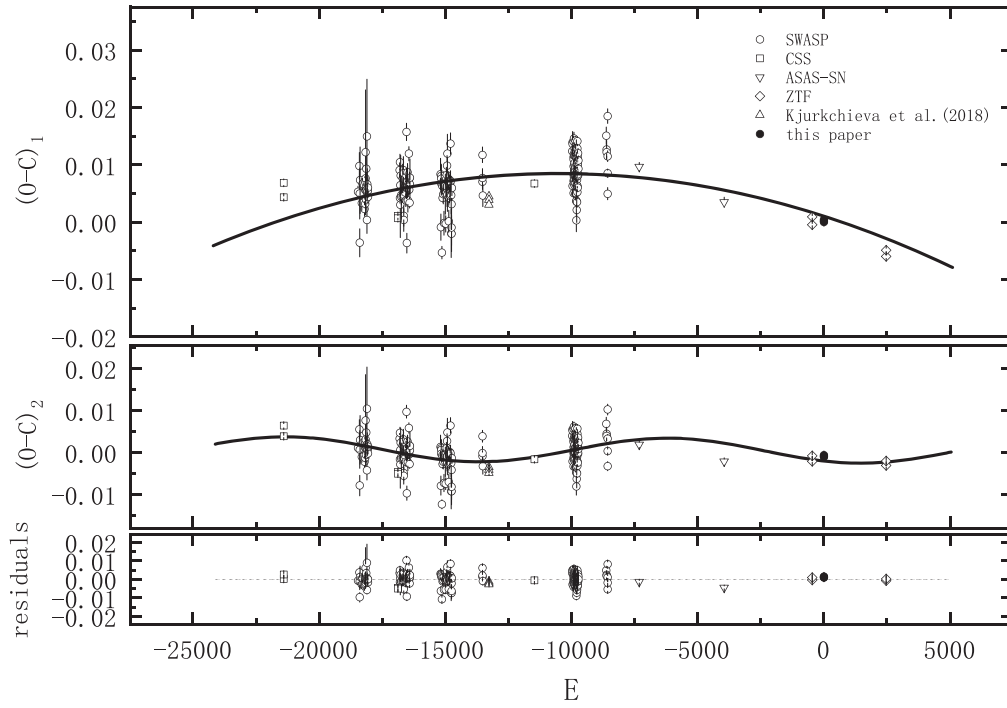


Figure 3. The  $O - C$  of V0644 Ser.

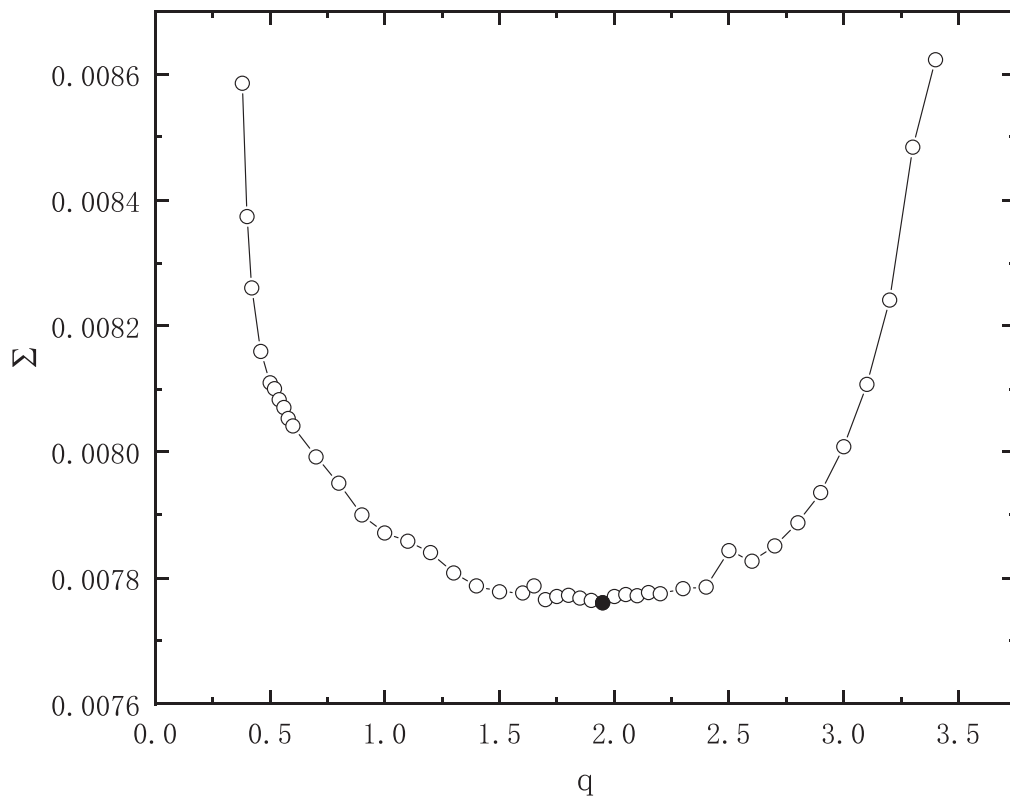
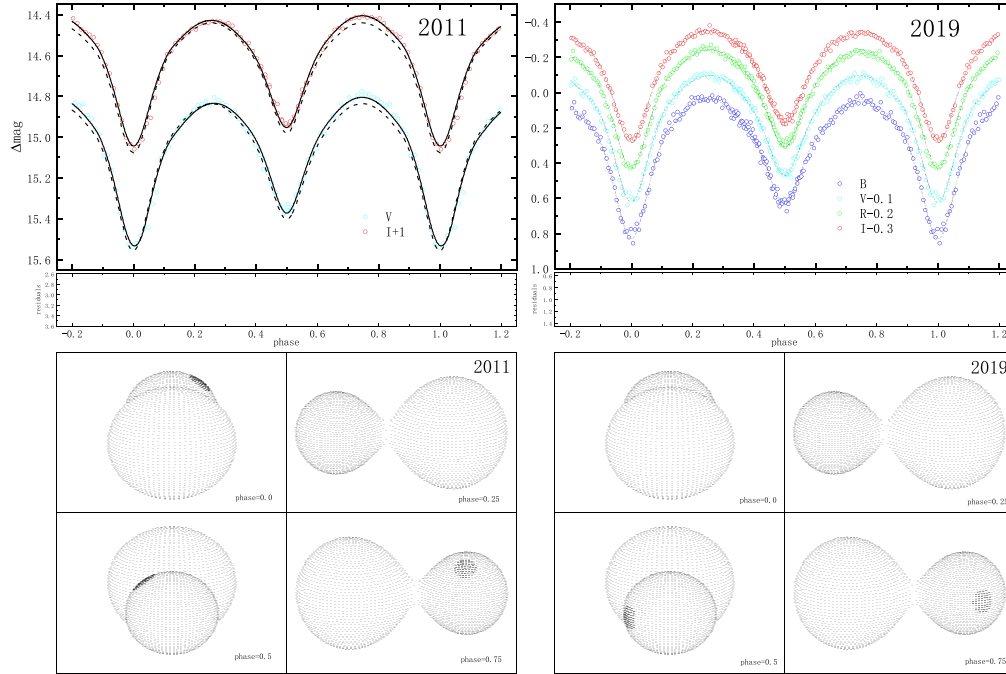


Figure 4. q-search graph of V0644 Ser.



**Figure 5.** Upper panel: The fitting curves of light curves in 2011 (left) and 2019 (right). The dotted lines are the fitting curve without spot, while the solid lines are the fitting curves with spot and third light. Lower panel: The geometric configuration of V0644 Ser with a spot in 2011 (left) and 2019 (right).

**Table 4**  
W-D Solutions of V0644 Ser

Parameters	combined solutions	2011 solutions	2019 solutions	Kjurkchieva et al. (2018)
$q$	1.95(2)	1.95(2)	1.95(2)	2.19(1)
$i$ (deg)	77.2(1)	77.2(1)	77.2(1)	79.1(1)
$T_1$ (K)	4750	4750	4750	4750
$T_2$ (K)/ $T_1$ (K)	0.953(1)	0.953(1)	0.953(1)	0.914(4)
$\Omega_1 = \Omega_2$	5.10(3)	5.10(3)	5.10(3)	5.28(4)
$L_{1B}/(L_{1B}+L_{2B})$	0.453(2)	0.453(2)	0.453(2)	...
$L_{1V}/(L_{1V}+L_{2V})$	0.432(2)	0.432(2)	0.432(2)	...
$L_{1R}/(L_{1R}+L_{2R})$	0.415(2)	0.415(2)	0.415(2)	...
$L_{1I}/(L_{1I}+L_{2I})$	0.404(2)	0.404(2)	0.404(2)	...
$r_1$ (pole)	0.3094(7)	0.3094(7)	0.3094(7)	...
$r_1$ (side)	0.3241(8)	0.3241(8)	0.3241(8)	...
$r_1$ (back)	0.3614(9)	0.3614(9)	0.3614(9)	0.344(3)
$r_2$ (pole)	0.418(3)	0.418(3)	0.418(3)	...
$r_2$ (side)	0.445(4)	0.445(4)	0.445(4)	...
$r_2$ (back)	0.475(6)	0.475(6)	0.475(6)	0.479(3)
$f$	0.14(4)	0.14(4)	0.14(4)	0.39
$\phi$ (deg)	...	0.703	1.573	...
$\theta$ (deg)	...	1.518	2.088	300
$r_s$	...	0.265	0.236	0.436
$T_s/T_p$	...	1.206	0.911	0.9
$L_{3B}/(L_{1B}+L_{2B}+L_{3B})$	...	...	...	...
$L_{3V}/(L_{1V}+L_{2V}+L_{3V})$	...	...	...	...
$L_{3R}/(L_{1R}+L_{2R}+L_{3R})$	...	...	0.006(4)	...
$L_{3I}/(L_{1I}+L_{2I}+L_{3I})$	...	0.016(7)	0.029(5)	...
$\Sigma$	0.00740	0.00329	0.00539	...



**Table 5**  
Physical Parameters of V0644 Ser

$M_1(M_\odot)$	$M_2(M_\odot)$	$R_1(R_\odot)$	$R_2(R_\odot)$	$L_1(L_\odot)$	$L_2(L_\odot)$	$A(R_\odot)$	$D(\text{pc})$
0.29(4)	0.56(9)	0.48(3)	0.65(3)	0.11(2)	0.16(2)	1.45(7)	439(6)

along with time. According to our results, the region went from hot to cool between 2011 and 2019, and we use change between the hot spot and the dark spot to equivalent this change. In general, the O'Connell effect can be explained by the spot on the surface of stars caused by magnetic activity. As we known that K- and M-type dwarfs have strong magnetic activity (Saar 1996, 2001). In addition, V0644 Ser is a shallow contact system, and its common envelope is thin, which means that convection can be unstable. Thus, a more likely explanation is the localized occurrence of regions of high or low temperature due to thermal instability caused by convection in the common envelope.

Combined with photometric solutions and parallax, the absolute parameters of the system can be estimated by the method described by Li et al. (2021b). Gaia gives a parallax  $\varpi$  as 2.2768 mas for V0644 Ser (Gaia Collaboration et al. 2018). It can be estimated that its distance is about 439 pc. The distance modulus of V0644 Ser can be calculated by the following formula,

$$(m - M)_v = 10 - 5lg\varpi + A_v, \quad (3)$$

where the extinction is 0.124 mag (determined by using the S and F method from the IRAS database, Schlafly & Finkbeiner 2011). Since the differential photometry method was used, with the apparent magnitude of the comparison star, we can obtain the apparent magnitude of V0644 Ser at maximum brightness in the V band as 14.92 mag. Thus, its absolute magnitude in the V band can be derived based on the distance modulus. Combined with the bolometric correction (e.g.,  $BC_v = -0.39$  mag for  $T = 4750$  K, Worthey & Lee 2011), the bolometric absolute magnitude can be obtained by Equation (4).

$$M_{\text{bol}} = M_v + BC_v. \quad (4)$$

Thus, the total luminosity  $L_T$  of the system is obtained by Equation (5).

$$L_T = L_1 + L_2 = 10^{-0.4(M_{\text{bol}} - 4.74)} \times L_\odot \quad (5)$$

According to Stefan–Boltzmann's law, we have

$$(L_1 + L_2)/L_\odot = (Ar_1)^2 \times \left(\frac{T_1}{T_\odot}\right)^4 + (Ar_2)^2 \times \left(\frac{T_2}{T_\odot}\right)^4, \quad (6)$$

where  $T_\odot$  represents the effective surface temperature of the Sun, with a value of 5780 K.  $r_1$  and  $r_2$  represent the relative radii of the star 1 and star 2 respectively, which can be obtained from the photometric solutions, i.e.,  $r_i = (r_{\text{ipole}} * r_{\text{iside}} * r_{\text{iback}})^{1/3}$ .

Then, the semimajor axis  $A$  is derived to be  $1.45 R_\odot$ . Finally, according to Kepler's third law and mass ratio,

$$\frac{A^3}{P^2} = 74.5(M_1 + M_2), \quad (7)$$

$$q = \frac{M_2}{M_1}, \quad (8)$$

two components masses  $M_1$  and  $M_2$  can be obtained. All the physical parameters are listed in Table 5, where the parameters with subscript 1 represent the parameters of the less massive star.

The photometric results of Kjurkchieva et al. (2018) are listed in column 5 of Table 4 for comparison. As can be seen from Table 4, our photometric results obtained by the W-D code are similar to those obtained by Kjurkchieva et al. (2018). The difference is that we get a lower contact degree, which means that V0644 Ser is a W-type shallow contact binary system. In addition, since the third light is only detected in the R and I bands, it may come from a late-type star.

#### 4.2. Period Variation

The  $O - C$  analysis results showed that the orbital period change of V0644 Ser has two parts: long-term period decrease and periodic oscillation. For the long-term period decrease, the possible explanation is that the orbital period of the system decreases due to AML via magnetic stellar wind and the mass transfer from the more-massive component to the less-massive one. We estimated the period decrease by AML via magnetic stellar wind from the following equation given by Bradstreet & Guinan (1994):

$$\dot{P}_{\text{AML}} \approx 1.1 * 10^{-8} * q^{-1} * (1 + q)^2 * (M_1 + M_2)^{-5/3} * k^2 * (M_1^* R_1^4 + M_2^* R_2^4) * P^{-7/3} \quad (9)$$

where  $k^2$  adopting a value of 0.1. The rate of period decrease due to spin-orbit coupled AML can be derived as  $\dot{P}_{\text{AML}} \approx 2.48 \times 10^{-8}$  days  $\text{yr}^{-1}$ . This rate is much slower than the rate of observed period decrease,  $\dot{P} = 2.23 \times 10^{-7}$  days  $\text{yr}^{-1}$ . Therefore, there is the mass transfer that dominates the long-term period decrease of V0644 Ser. The mass transfer rate can be calculated according to the following equation,

$$\frac{\dot{P}_m}{P} = 3 \left( \frac{M_2}{M_1} - 1 \right) \frac{\dot{M}_2}{M_2} \quad (10)$$

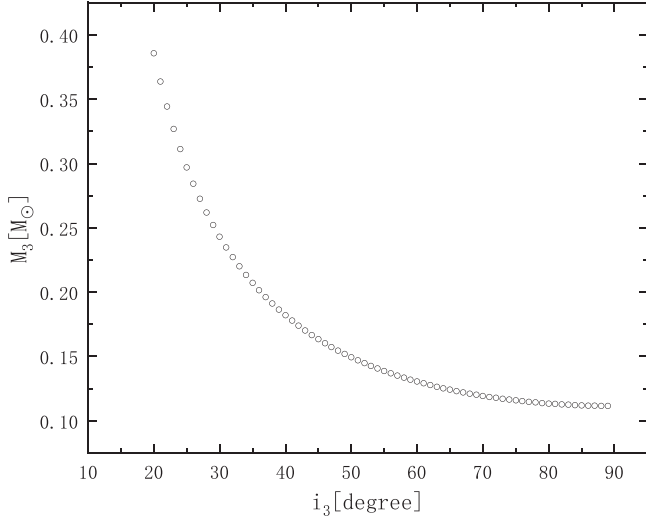


**Figure 6.** The relationship between the mass of third body and orbital inclination.

where  $\dot{P}_m = \dot{P} - \dot{P}_{\text{AML}}$ ,  $M_1$  and  $M_2$  were derived from the previous section. Therefore, the mass transfer rate was obtained as  $1.80 \times 10^{-7} M_{\odot} \text{ yr}^{-1}$ . As the orbital period shrinks, the system will evolve toward the deeper contact stage. On the other hand, Qian (2003) suggested that the W-type contact binaries oscillated around a critical mass ratio by the combination of the TRO and the AML via a change of depth of the contact. Recently, Zhang et al. (2020) investigated the overluminescence of the W-type contact binary system of secondary component and believed that the W-type was in the stage of the thermal relaxation oscillation. Then the orbital period of V0644 Ser may decrease to some critical value and then increase again.

For the periodic oscillation, Liao & Qian (2010) discovered that the most plausible explanation of the cyclic period changes is the light travel time effect caused by the third body in EW-type binaries. This is also consistent with the third light found in the light curves analysis. The mass function of the third body can be calculated by the following equation,

$$f(m) = \frac{4\pi^2}{GT^2} \times (a'_{12} \sin i_3)^3 = \frac{(M_3 \sin i_3)^3}{(M_1 + M_2 + M_3)^2} \quad (11)$$

Here,  $M_3$  is the mass of the third body. The relationship between the orbital inclination and the corresponding mass of the third body is plotted in Figure 6. The parameters of the third body are listed in Table 6. The minimum mass of the third body is  $0.11 M_{\odot}$  ( $i_3 = 90^\circ$ ). Combined with the third light contribution found in the *R* and *I* bands in photometric solutions, it is speculated that the third body is a cool star.

Some ultrashort period contact binary systems have also been detected the presence of third body based on orbital period analysis, such as SDSS J001641-000925 (Qian et al. 2015),

**Table 6**  
Parameters of the Third Component for V0644 Ser

Parameters	Values
$\omega$ ( $^\circ$ )	0.024(1)
$K$ (d)	0.0029(1)
$P_3$ (y)	9.15(3)
$a_{12} \sin i$ (au)	0.50(2)
$f(m)$ ( $M_{\odot}$ )	0.0015(2)
$M_3(i_3 = 90^\circ)$ ( $M_{\odot}$ )	0.112(6)
$a_3(i_3 = 90^\circ)$ (au)	3.8(4)

DY CVn (ZhiNing et al. 2017), ISWASP J161335.80-284722.2 (Fang et al. 2019), V574 Lyr (Long et al. 2019), etc. According to the period-color relation (Eggen 1967; Qian et al. 2020), the ultrashort period contact binaries usually composed of low-mass star of K- or M-type. They evolve very slowly because of their main sequence stage is very long, and their AML timescale is longer than the Hubble time (Stepien 2006, 2011). Therefore it is difficult to form such contact binary systems. But some of these systems have been observed. The third body may play an important role to their formation. Combining our new light curves and *O* – *C* analysis, we found that the V0644 Ser is a triple system. This third body is a cool star, and it may play a crucial role to form the present contact binary V0644 Ser by removing the angular momentum in order to decrease the AML timescale. Since ultrashort period contact binaries remain rare, more of such binaries should be observed and studied in the future to reveal their mysteries.

### Acknowledgments

Special thanks to Prof. Andrew Norton for the SuperWasp Sky Survey data. This work was supported by the National Natural Science Foundation of China (Nos. 11922306 and 11933008). We acknowledge the use of 85 cm telescope in Xinglong station of National Astronomical Observations, Chinese Academy of Sciences.

### ORCID iDs

Sarotsakulchai Thawicharat  <https://orcid.org/0000-0001-8546-5875>

### References

- Binnendijk, L. 1970, *VA*, **12**, 217
- Bradstreet, D. H., & Guinan, E. F. 1994, in ASP Conf. Ser. 56, *Interacting Binary Stars*, ed. A. W. Shafter (San Francisco, CA: ASP), 228
- Davenport, J. R. A., Becker, A. C., West, A. A., et al. 2013, *ApJ*, **764**, 62
- Dimitrov, D. P., & Kjurkchieva, D. P. 2015, *MNRAS*, **448**, 2890
- Drake, A. J., Graham, M. J., Djorgovski, S. G., et al. 2014, *ApJS*, **213**, 9
- Eggen, O. J. 1967, *MmRAS*, **70**, 111
- Fang, X.-H., Qian, S., Zejda, M., et al. 2019, *PASJ*, **71**, 125
- Flannery, B. P. 1976, *ApJ*, **205**, 217

- Gaia Collaboration, Brown, A. G. A., Vallenari, A., et al. 2018, *A&A*, **616**, A1
- Graham, M. J., Kulkarni, S. R., Bellm, E. C., et al. 2019, *PASP*, **131**, 078001
- Jiang, D., Han, Z., Ge, H., Yang, L., & Li, L. 2012, *MNRAS*, **421**, 2769
- Kjurkchieva, D., Popov, V., Vasileva, D., & Petrov, N. 2016, *SerAJ*, **192**, 21
- Kjurkchieva, D. P., Dimitrov, D. P., Ibryamov, S. I., & Vasileva, D. L. 2018, *PASA*, **35**, e008
- Kopal, Z. 1959, *Close Binary Systems* (London: Chapman & Hall)
- Li, K., Kim, C.-H., Xia, Q.-Q., et al. 2020, *AJ*, **159**, 189
- Li, K., Xia, Q.-Q., Kim, C.-H., et al. 2021a, *ApJ*, **922**, 122
- Li, K., Xia, Q.-Q., Kim, C.-H., et al. 2021b, *AJ*, **162**, 13
- Li, K., Xia, Q.-Q., Michel, R., et al. 2019, *MNRAS*, **485**, 4588
- Liao, W. P., & Qian, S. B. 2010, *MNRAS*, **405**, 1930
- Lohr, M. E., Norton, A. J., Kolb, U. C., et al. 2013, *A&A*, **549**, A86
- Long, L., Zhang, L.-Y., Han, X. L., et al. 2019, *MNRAS*, **487**, 5520
- Lucy, L. B. 1968, *ApJ*, **151**, 1123
- Lucy, L. B. 1976, *ApJ*, **205**, 208
- Masci, F. J., Laher, R. R., Rusholme, B., et al. 2019, *PASP*, **131**, 018003
- O'Connell, D. J. K. 1951, *MNRAS*, **111**, 642
- Qian, S. 2003, *MNRAS*, **342**, 1260
- Qian, S.-B., He, J.-J., Zhang, J., et al. 2017, *RAA*, **17**, 087
- Qian, S. B., Jiang, L. Q., Fernández Lajús, E., et al. 2015, *ApJL*, **798**, L42
- Qian, S.-B., Zhu, L.-Y., Liu, L., et al. 2020, *RAA*, **20**, 163
- Robertson, J. A., & Eggleton, P. P. 1977, *MNRAS*, **179**, 359
- Rucinski, S. M. 1992, *AJ*, **103**, 960
- Saar, S. H. 1996, in *Stellar Surface Structure*, ed. K. G. Strassmeier & J. L. Linsky, Vol. 176 (Dordrecht: Kluwer), 237
- Saar, S. H. 2001, in *ASP Conf. Ser. 223*, 11th Cambridge Workshop on Cool Stars, Stellar Systems and the Sun, ed. R. J. Garcia Lopez, R. Rebolo, & M. R. Zapaterio Osorio (San Francisco, CA: ASP), 292
- Schlafly, E. F., & Finkbeiner, D. P. 2011, *ApJ*, **737**, 103
- Shappee, B., Prieto, J., Stanek, K. Z., et al. 2014, *AAS Meeting Abstracts*, 223, 236.03
- Stepien, K. 2006, *AcA*, **56**, 347
- Stepien, K. 2011, *AcA*, **61**, 139
- Van Hamme, W. 1993, *AJ*, **106**, 2096
- Wilson, R. E. 1979, *ApJ*, **234**, 1054
- Wilson, R. E. 1990, *ApJ*, **356**, 613
- Wilson, R. E. 1994, *PASP*, **106**, 921
- Wilson, R. E., & Devinney, E. J. 1971, *ApJ*, **166**, 605
- Worthey, G., & Lee, H.-c 2011, *ApJS*, **193**, 1
- Zhang, X.-D., & Qian, S.-B. 2020, *MNRAS*, **497**, 3493
- Zhang, X.-D., Qian, S.-B., & Liao, W.-P. 2020, *MNRAS*, **492**, 4112
- ZhiNing, Q., LinQiao, J., Jie, L., YanFei, H., & YuQuan, Y. 2017, *NewA*, **54**, 103